Dwarfs Cooler Than "M": The Definition of Spectral Type "L" using Discoveries from the 2-Micron All-Sky Survey (2MASS)[1]

J. Davy Kirkpatrick
Infrared Processing and Analysis Center, M/S 100-22, California Institute of Technology, Pasadena, CA 91125; davy@ipac.caltech.edu

I. Neill Reid
Palomar Observatory, M/S 105-24, California Institute of Technology, Pasadena, CA 91125

James Liebert
Steward Observatory, University of Arizona, Tucson, AZ 85721

Roc M. Cutri, Brant Nelson, Charles A. Beichman
Infrared Processing and Analysis Center, M/S 100-22, California Institute of Technology, Pasadena, CA 91125

Conard C. Dahn, David G. Monet
U.S. Naval Observatory, P.O. Box 1149, Flagstaff, AZ 86002
and

John E. Gizis, Michael F. Skrutskie
Five College Astronomy Department, Department of Physics and Astronomy, University of Massachusetts, Amherst, MA 01003

class T
low mass
brown dwarf
stellar atmosphere

ABSTRACT

Before the 2-Micron All-Sky Survey (2MASS) began, only six objects were known with spectral types later than M9.5 V. In the first 371 sq. deg. of actual 2MASS survey data, we have identified another twenty such objects spectroscopically confirmed using the **Low Resolution Imaging Spectrograph** (LRIS) at the W. M. Keck Observatory. Because the TiO and VO bands which dominate the far-optical portions of late-M spectra disappear in these cooler dwarfs, we define a new **spectral class** — "L" — where metallic oxides are replaced by **metallic hydrides** and **neutral alkali metals** as the major spectroscopic signatures. We establish classification indices and type all twenty-five L

[1]Portions of the data presented herein were obtained at the W.M. Keck Observatory which is operated as a scientific partnership among the California Institute of Technology, the University of California, and the National Aeronautics and Space Administration. The Observatory was made possible by the generous financial support of the W.M. Keck Foundation.

dwarfs. The twenty-sixth "post-M9.5" object - Gl 229B - is the prototype of a methane-dominated spectral class which we propose as class "T".

At least five of the twenty 2MASS L dwarfs show the 6708-Å lithium doublet *at low resolution*, the strongest having an equivalent width of 18.5 Å. For objects this cool, the presence of lithium proves that they are substellar. Two other 2MASS objects appear to have lithium lines at the limit of our detectability which if verified means that at least a third of our L dwarfs are bona fide brown dwarfs. All of the 2MASS brown dwarfs discovered so far have J-K_s > 1.30. We have not yet, despite deliberately searching for them, found any brown dwarfs with colors resembling Gl 229B ($J - K_s \approx -0.1$).

Subject headings: stars: low-mass, brown dwarfs — stars: fundamental parameters — infrared: stars — stars: atmospheres — stars: distances

having no optical counterpart and $J-K_s \leq 0.40$, were either identified by the 2MASS processing pipeline as known asteroids or flagged by hand as high proper motion objects already tabulated in the LHS Catalog (Luyten 1980). Thus, all of our brown dwarf suspects with $J-K_s \leq 0.40$ were eliminated immediately so none required spectroscopic follow-up. Identifications for these objects are given in column 6 of Table 1B along with the observation date (in column 7) of the 2MASS scan in which it was found. These objects will not be discussed further.

Several other objects not meeting the standard search criteria (not red enough to meet the $J-K_s \geq 1.30$ criterion or falling outside the 371 sq. deg. search area) were also observed and are listed in the top portion of Table 2. Several late dwarfs selected from the literature and serving as comparisons were also observed. These are listed in the bottom portion of Table 2. The column descriptions are the same as in Table 1A.

3. Follow-up Observations

Targets in Table 1A and Table 2 were followed up using the Low Resolution Imaging Spectrograph (LRIS; Oke et al. 1995) at the 10m W. M. Keck Observatory on Mauna Kea, Hawaii. A 400 g/mm grating blazed at 8500 Å was used with a 1″ slit and 2048×2048 CCD to produce 9-Å-resolution spectra covering the range 6300 – 10100 Å. Objects were observed during three separate observing runs on 1997 Nov 08, 09 (UT), 1997 Dec 07, 08, 09 (UT), and 1998 Jan 22, 23, 24 (UT). Most of the run on 1997 Nov 08 (UT) was lost because of fog, but the other seven nights were photometric with generally excellent seeing (between 0.″6 and 0.″8 FWHM). Observations dates and exposure times for each target are given in columns 6 and 7 of Tables 1A and 2.

During the Dec and Jan runs, we used the OG570 order-blocking filter to eliminate second-order light. We erroneously used the GG495 filter during the Nov run, but because our targets are all extremely red with very little measureable flux below 6000 Å, the poor choice of filter only affected the much bluer flux calibration standards and only at wavelengths beyond 9900 Å. This effect was relatively easy to correct since we have the same flux standards taken with the correct OG570 filter in subsequent runs.

The data were reduced and calibrated using standard IRAF routines. A 1-second dark exposure was used to remove the bias, and quartz-lamp flat-field exposures were used to normalize the response of the detector. The individual stellar spectra were extracted using the "apextract" routine in IRAF, allowing for the slight curvature of a point-source spectrum viewed through the LRIS optics and using a template where necessary. Wavelength calibration was achieved using neon+argon arc lamp exposures taken after each program object. Finally, the spectra were flux-calibrated using observations of standards LTT 9491, Hiltner 600, and LTT 1020 from Hamuy et al. (1994).

Classifications based on the resulting spectra are given in column 8 of Tables 1A and 2. With one exception, all of the objects between RA=03^h26^m and 03^h30^m are background stars heavily reddened by intervening molecular clouds in Perseus. For M dwarfs, spectral types were assigned using the least-squares minimization technique described in Kirkpatrick et al. (1991) using spectral standards previously observed at similar resolutions and over the same wavelengths as those described here. For M dwarfs of type M7 and later, these types were refined using the VO ratio described in Kirkpatrick et al. (1997b).

All dwarfs later than spectral type M9.5 are discussed in the next section, and notes on individual M9.5+ dwarfs can be found in Appendix A. Notes on other interesting objects can be found in Appendix B.

4. Results for Dwarfs Cooler Than Type M9.5 V

Listed in Table 3 are all the dwarfs from Tables 1A and 2 which have spectral types cooler than M9.5 V. This includes the 2MASS dwarf discovered in Prototype Camera data (Kirkpatrick et al. 1997a), Kelu-1 discovered during the course of the proper motion survey of Ruiz et al. (1997), and the three cool dwarfs discovered by the DEep Near Infrared Survey (DENIS; Delfosse et al. 1997; Tinney et al. 1997). Also included in the table for comparison purposes are the only two companion objects currently known with spectral types cooler than M9.5 V – GD 165B and Gl 229B. In total, 26 dwarfs have been found with post-M9.5 types, and 20 of those are from 2MASS. Optical and near-infrared finder charts for the 2MASS objects are shown in Figure 2.

Spectra for each of the objects in Table 3 are shown in Figure 3. These are ordered in temperature from the warmest at top left to the coolest at bottom right. Two of these spectra are shown in detail in Figure 4

warfs dominated by CaH and MgH bands. Like "L", "H" is not currently in use and would be a recycling of a previous Fleming class.

• "T" or "Y" – If we take the position of purists and say that letters should not be recycled, then this leaves only "T" and "Y". This stance, however, leaves very little room for extending the sequence further. We already know of one cooler object (Gl 229B) which does not fit into the new spectral sequence because it is so much colder than the others. Its spectrum is dominated by methane, much like the Jovian planets. Hence, once we have enough objects similar to Gl 229B, they too will require a new letter since they are fundamentally different from the dwarfs discussed here.

Because "L" has a slight edge over "H" and both are preferred to "T" or "Y", we will adopt "L" as the class for the new objects[5]. For cooler spectra, we will attempt to go in alphabetical order from "L", thus making "T" the class for the methane-dominated spectra of the Gl 229B-type.

Over the past several months, class "L" has been floated as the new letter in several colloquia and scientific meetings, and there appears to be no strong objection to "L" within the astronomical community. We must re-emphasize, however, that "L" does not carry any meaning – these objects should not be referred to as *lithium* dwarfs since at least two-thirds show no lithium at low resolution (see §7) or *low*-luminosity dwarfs since Gl 229B (a non-L) is lower in luminosity. Because some of these objects *are* substellar and thus not truly stars, the entire collection should be referred to as "L dwarfs", not "L stars". This will also eliminate any confusion with L* galaxies. So that these new spectral types are more recognizable *as* spectral types, we will append a luminosity class "V" on them even though L-class objects do not exist for other luminosity classes such as III or I.

As another consideration on choice of letter, it should be noted that as the giant sequence has been pushed to cooler temperatures, M types have been retained. Giant classes M10 and M11 are sometimes seen in the literature (Bessell 1991). These objects are still dominated by strong bands of TiO and VO, so it is reasonable to continue the M sequence to higher numbers. Some critics have argued that the latest M types break with the tradition of the standard Morgan, Keenan, & Kellman (1943) system, which stipulates that objects of the same spectral class but different luminosity classes have essentially identical temperatures. Bessell (1991), in attempting to force this requirement on the classification of the latest M dwarfs, advocates a system which collapses the Boeshaar & Tyson (1985) types M7 through M9 into a single subclass.

However, the difference in luminosity between late-M dwarfs and giants exceeds five orders of magnitude and the surface gravities also differ by five orders of magnitude. Thus, the physical processes which dominate dwarf and giant spectra will be clearly dissimilar. Forcing the late-M dwarfs to follow the same mapping of temperature into spectral type as the late-M giants is unnecessary. Besides, dwarfs of classes M7, M8, and M9 have distinct taxonomic differences and should not be relegated to a single subtype. Therefore we will retain the late-M dwarf classification of Boeshaar & Tyson as further refined by Kirkpatrick et al. (1991) and Kirkpatrick et al. (1997b) and use those as a starting point for the L-dwarf sequence.[6]

[5] Martín et al. (1997) have also noted that "L" would be a good choice of letter. We disagree, however, with their suggestion that the L class be divided into L_{Li} and L_{CH_4} categories since the onset of methane – because it changes the near-infrared spectrum of Gl 229B so dramatically from the L dwarfs (Figure 5) – justifies a new class in its own right. The emphasis of Martín et al. seems to be in distinguishing brown dwarfs from stars, and this is further reflected in their suggestion to create new M classes with designations like "bdM$_{Li}$". The problem here is that the lithium line is often very weak, so in order to assign a class accurately, we would need both low resolution spectra to assign temperature subclasses 0, 1, 2, etc. and high resolution spectra to assign the *Li* subscript. Furthermore and more importantly, not all brown dwarfs have lithium and not all M dwarfs with lithium are substellar. Creating a taxonomy for these objects which mixes spectral features with our (current) understanding of the physics should, as stated earlier, be avoided.

[6] Perhaps the last consideration in selecting a new spectral class is choosing the new mnemonic. Many introductory astronomy texts use the phrase "Oh Be A Fine Girl/Guy, Kiss Me" to aid students in remembering the correct OBAFGKM sequence of spectral types. We must now augment the mnemonic with "...Kiss Me, Love" or "...Kiss My Lips", both of which keep the cadence of the original by adding another monosyllabic word for "L". However, the inclusion of spectral type T would require an augmentation such as "...Kiss My Lips, Tom". One astronomer, upon hearing of spectral class L, countered with "Only Borish Astronomers Find Girl Kissing Mnemonics Likeable". This having been said, we will leave the establishment of the new mnemonic as an exercise for the astronomical community as a whole.

data were already bad-pixel masked, flat-fielded, sky-subtracted, and coadded into a single ABBA image. Spectra were then extracted using the apextract package of IRAF. Spectra and their corresponding arcs were extracted using identical traces along the array. The extractions were then wavelength calibrated and corrected for telluric absorption by dividing by the A-type spectra standard taken at a similar airmass.[8] Flux calibration was obtained by assuming the A-type standards are blackbodies at the temperatures inferred from their published spectral types. Finally, the individual ABBA spectra were summed into one final spectrum for each target, and the flux scaling of this final spectrum normalized to one at 2.20 μm.

The resulting spectra are shown in Figure 5. For comparison, the Gl 229B spectrum of Geballe et al. (1996) — also acquired with CGS4 on UKIRT — is shown as well. Both of the 2MASS spectra show CO bandheads and no trace of CH_4. Thus, we believe that the feature seen in the Delfosse et al. spectrum of DENIS-P J0205.4−1158 is not attributable to methane either, since that object's optical spectrum shows that it is intermediate in temperature between the two 2MASS objects displayed in Figure 5.

5.2.3. Establishing the Grid of Subclasses

The conclusion from Fig. 5, then, is that we have yet to detect the onset of methane absorption at 2.2 μm in the 2MASS discoveries. This is consistent with the fact that the 2MASS $J-K_s$ colors are, with some cosmic scatter, increasing with cooler types. (Refer to §6.1 and Figure 13 for more on this.) Once methane has appeared at K_s-band, we would expect the $J-K_s$ color to turn bluer, as it does in Gl 229B.

It should be noted here that the search for infrared-selected QSOs (Cutri et al. 1998) has identified candidates over a larger area of sky than that surveyed here (~1900 sq. deg., or roughly five time as much coverage as our survey), and only a dozen additional IR-only sources with $J-K_s > 2.00$ were found beyond those listed in Tables 2 and 3. Of those not already followed up, only two have $J-K_s > 2.10$ and one of these has $J-H$ and $H-K_s$ colors incompatible with other L dwarfs. In other words, L dwarfs redder in $J-K_s$ than our coolest example have not been found despite a much larger search. Thus, we believe that we already have objects near the breakpoint between classes L and T and that objects with temperatures cooler than 2MASS J1632291+190441 will also have $J-K_s$ colors less than ~2.00 or perhaps considerably less than ~2.00 depending upon how quickly the onset of methane absorption occurs with temperature. However, to leave room for additional L types in case cooler non-methane objects are discovered, we will set the spectral type of 2MASS J1632291+190441 to be L8 V.

Table 6 establishes qualitative spectral diagnostics which define each subclass from L0 through L8. Also listed in the table is a bright representative object for each subclass. These objects can be regarded as the primary spectral standards. Figure 6, a subset of Figure 3, serves as a visual guide to Table 6 by showing these primary standards in greater detail and comparing them to spectra of late-M dwarfs and the only known T-dwarf. Figure 7 shows blow-ups of the spectra from 7300 – 8000 Å and 8400 – 9000 Å to help further illustrate the criteria of Table 6.[9]

As one final note about defining the latest L subclasses, it is reasonable to imagine, after looking at Figures 6 and 7, that an L9 dwarf would have imperceptible FeH bands and much weaker CrH bands than the L8 dwarf 2MASS J1632291+190441. Once these hydrides have disappeared from the far optical spectra, the result will be an almost smooth spectrum much like that of the methane brown dwarf Gl 229B shown at the bottom of Figures 6 and 7. This lends support to our belief that the coolest known L dwarfs are only slightly warmer than the temperature at which methane forms.

5.2.4. Spectral Ratios

In choosing classification diagnostics, we will use spectral ratios like those devised by Kirkpatrick et al. (1991). These ratios are a measure of the summed flux in a region containing a line or band of interest divided into the summed flux in a nearby region approximating the local pseudo-continuum. In Table 7 we give the name of the ratio (column 1), the regions used in the summing (columns 2 and 3), and the fea-

[8] There are residuals in the final spectra due to 1.817 μm Brϵ, 1.875 μm Paα, and 1.944 μm Brδ absorptions in the A-type star because these could not be disentangled from the deep telluric absorption between 1.80 and 1.95 μm. Other stellar absorptions in the A-type star were removed before division.

[9] It should be noted that a few late dwarfs previously assigned "≥M" designations in Kirkpatrick et al. (1995, 1997b) can now have final designations assigned. LP 944-20 is type M9 V, BRI 0021-0214 is type M9.5 V, and PC 0025+0447 is M9.5 V (peculiar).

are shown for comparison.[11] Also shown is the location of the only known T dwarf, Gl 229B. The plot shows that the $J - K_s$ color is, with some cosmic scatter, monotonically increasing with later type from late-M through late-L then turns dramatically bluer for Gl 229B once methane absorption starts to dominate the K_s-band measurement.

Using the absolute flux calibration of the Keck spectra, we can derive rough I-band measurements for each of the L dwarfs as well. Specifically, we have taken a simple square bandpass with beginning and end points lying at the half-power points of the I_C band (7250 and 8750 Å; Bessell 1979) and have calculated the average flux in units of F_ν (ergs/cm^2 s Hz) in the bandpass. Using a zero-point flux of 2550 Jy for the I_C filter (Berriman & Reid 1987), we have converted these fluxes to magnitudes and listed the results along with the $I - K_s$ colors in columns 6 and 7 of Table 3. The $I - K_s$ color is shown as a function of spectral type in Figure 13b, again with late-M dwarfs and Gl 229B for comparison. Note that $I - K_s$ increases fairly monotonically with spectral type for L dwarfs, meaning that a crude type can be assigned based on the $I - K_s$ color alone. However, this trend reverses by the time temperatures like that of Gl 229B are encountered.

The 2MASS color can also be used to plot L dwarfs on the familiar $J - H$ vs. $H - K_s$ diagram. This is shown in Figure 14. For illustration, M dwarfs from Leggett (1992) are also plotted together with Gl 229B and the tracks for giants (dashed line) and dwarfs (solid line) from Bessell & Brett (1988). For the most part, L dwarfs lie on a redward extension of the well-known dwarf track.[12] Note however the position of Gl 229B on the opposite side of the diagram from the L dwarfs.

6.2. Hα Emission

Several of the L dwarfs in Table 3 exhibit Hα in emission. Equivalent width (hereafter, EW) measures are listed in column 3 of Table 9 and are plotted as a function of spectral class in Figure 15a. Those spectra with clear or possible Hα emission are shown in Figure 16. The coolest object with measurable Hα, 2MASS J0326137+295015, also has the strongest line — 9.1 Å EW.[13]

6.3. Lithium Absorption

Seven of the 25 L dwarfs show the Li I 6708-Å line in our LRIS spectra. Two of these are previously known brown dwarfs — Kelu-1 and DENIS-P J1228.2−1547. The other five are all 2MASS discoveries. Two other 2MASS L dwarfs may have lithium at our detection limit. Equivalent width measures are listed in column 4 of Table 9 and are plotted as a function of spectral type in Figure 15b. Those spectra with clear or possible lithium signatures are shown in Figure 17. Note that two of the 2MASS objects have Li I in excess of 15 Å EW. Lithium is discussed more fully in §8.3.

6.4. Rubidium and Cesium Absorption

Fig. 15c and 15d show the equivalent width measurements for Rb I and Cs I as a function of spectral class. Values are listed in columns 5 and 6 of Table 9. For Rb I, only the line at 7948 Å was measured since the line at 7800 Å falls in a low signal-to-noise region in the latest L dwarfs, making the EW measurements here more uncertain. For Cs I, only the line at 8521 Å was measured since the line at 8943 Å is severely contaminated by telluric absorption. For both rubidium and cesium, the EWs are seen to increase for cooler L dwarfs, making these excellent measures of spectral type. However, measuring these EWs is possible only because these spectra have good signal-to-noise and because these two lines lie in fairly unconfused regions of the spectrum where a pseudo-continuum can be readily determined. For general classification, the composte alkali-oxide ratios described in §5.2.4 should be used instead.

7. Trigonometric Parallaxes for L Dwarfs

Five of the objects in Table 3 have measured trigonometric parallaxes. Two of these have been previously published (GD 165B and Gl 229B), but the other three are new results from the USNO paral-

[11] These publications list K_{CIT} photometry, not K_s. However, Persson et al. (1998) have shown that for late M dwarfs the difference between K and K_s is negligible.

[12] The points for 2MASS J1439409+182637 and 2MASS J1334062+194034 lie outside the locus defined for the other L dwarfs. It is not yet known if this is a real effect or simply an indication of H-band photometry possibly biased by strong OH airglow in the 2MASS measurements.

[13] However, the M9.5 dwarf 2MASS J0149090+295613 is only slightly warmer than the earliest L dwarf and it has been observed during a massive flare in which the Hα EW was hundreds of Angstroms. See Appendix B for more on this object.

8.2. The Temperature Scale for L Dwarfs

Using the spectral diagnostics shown in Figures 9-11 along with the atmospheric properties predicted by Burows & Sharp (1998), a rough *ab initio* temperature scale can be assigned to the L spectral sequence. Table 11 gives the major spectroscopic features (column 1) seen in the spectra of Figures 4 and 5 and indicates where in spectral type the feature reaches maximum strength (column 2) and where it disappears from the observed spectra (column 3). In column 4 is listed the theoretical reason why the feature disappears, and column 5 gives the temperature at which it is expected to vanish from the spectrum. Generally, these disappearances are triggered by depletion into grains (for the molecules) or by formation into a chloride compound (for the alkali atoms). The rows of Table 11 are ordered so that features which are observed to disappear at the warmest temperatures are listed at the top, and those disappearing at cooler temperatures are at the bottom.

The first feature to disappear is titanium oxide. It slowly vanishes from the photosphere as it condenses into grains of perovskite ($CaTiO_3$). All bands of TiO have disappeared by L2 V except for the one at 8432 Å. As seen in Table 4, this band is the only TiO band *not* arising from the $A^3\Phi - X^3\Delta$ transition. Presumably, this transition originates at deeper layers in the photosphere and is the last to vanish as the photosphere becomes more transparent, largely through the disappearance of TiO at higher levels. This change in the physical location of the photosphere ($\tau = 1$) makes it difficult to ascribe the spectral type at which TiO truly disappears. Nonetheless, the observed maximum in TiO absorption around M7-8 V suggests that the 2300-2000 K regime lies at somewhat later spectral types, probably very early L.

Vanadium oxide is a little less problematic. After reaching a maximum at ~M9.5 V, it vanishes from the spectrum by ~L4 V after depleting onto solid VO.[14] Thus, L4 V roughly marks the 1700-1900 K regime.

The next feature to weaken and disappear is Na I. After reaching a maximun in the M dwarfs, sodium disappears entirely by ~L8 V. Burrows & Sharp indicate that sodium forms into NaCl at temperatures around 1150 K, but our spectra show that it disappears at much warmer temperatures well before NaCl is created. Instead, sodium may first disappear into high albite ($NaAlSi_3O_8$) at temperatures around 1200-1300 K as suggested by Figure 3 of Burrows & Sharp. If so, this fits in better with the other temperature predictions.

Moving to later types and cooler temperatures, the next feature to weaken is iron hydride, but this molecule is unfortunately not included in the Burrows & Sharp calculations. Chromium hydride, which is included in the models, follows, and it weakens markedly between types L5 and L8. This suggests that its predicted disappearance at ~1400 K corresponds to a type (yet to be defined) just cooler than L8 V.

The remaining features of L dwarf spectra — Li I, CO, Rb I, Cs I, K I, and H_2O — are not seen to vanish in the L sequence. Carbon is still predominantly found in carbon monoxide, not methane, so an L8 dwarf must be above 1200-1500 K. Rubidium, cesium, and potassium are all still visible, indicating that they have yet to form their chlorides. This means that an L8 dwarf must be warmer than 1200 K. Finally, water is still present in the optical and near-infrared spectra, not having yet condensed into clouds and dropped below the photosphere (as water has apparently done in the atmosphere of Jupiter). However, this occurs at much lower temperatures (~350 K). Lithium is discussed in detail in §8.3.

Given the above arguments, we can state that the L dwarf sequence represents temperatures from somewhere above 2000 K for L0 V down to ~1400 K for L8 V.

However, the use of molecular equilibrium diagnostics is more complicated than simply equating these temperatures to the effective temperature of the star, as illustrated by application of these ideas to Gl 229B with $T_{eff} \approx 950$K. The fact that Gl 229B shows CO in the near-IR and atomic Cs I lines in the far optical (Oppenheimer et al. 1998) demonstrates this point. Cesium and carbon monoxide should not exist in this form at this temperature, and the apparent solution is that mixing in the atmosphere of Gl 229B pulls up Cs I and CO from hotter layers below. On the other hand, because the L dwarf spectral signatures are so well correlated with predictions, this probably means that these objects – unlike Gl 229B and Jupiter – have stable radiative zones.

[14] Admittedly though, since VO lacks a sharp bandhead, its disappearance is a little more difficult to ascertain. However, the ~7950-Å inflection point in the spectrum of late-M and early-L dwarfs is caused by VO, and this inflection has vanished by L4 V.

• GD 165B (L4 V) - The prototype of the L dwarf class (Kirkpatrick et al. 1993), this object was discovered by Becklin & Zuckerman (1988) as the companion to a white dwarf. The separation between components is 4″. See Kirkpatrick et al. (1998) for a current review of this object.

• DENIS-P J1228.2−1547 (L5 V) - Discovered by Delfosse et al. (1997) and later shown to have lithium by Tinney et al. (1997) and Martín et al. (1997), this object shows a lithium line with an EW of 3.1 Å in our spectrum. The object has also been rediscovered in 2MASS data from the southern hemisphere, where it carries the designation of 2MASS J1228152−154734. The position encoded into this designation is more accurate than that provided by Delfosse et al. (1997).

• 2MASS J1553214+210907 (L5.5 V) - This object shows the strongest lithium line ever seen in a brown dwarf — the EW is 18.5 Å.

• 2MASS J0850359+105716 (L6 V) - This object also shows a remarkably strong lithium line with an EW of 15.2 Å. The LRIS guider camera at Keck showed a second component, with separation of <2″ at $PA = 82°$, but the spectrum confirms that this secondary is a background M dwarf. The K-band spectrum of the brown dwarf (Figure 5) shows clear CO absorption and strong H_2O bands.

• DENIS-P J0205.4−1159 (L7 V) - Also discovered by Delfosse et al. (1997), this object has been scanned by 2MASS where it carries the designation 2MASS J0205293−115930. The USNO parallax places it at 16.6 pc.

• 2MASS J1632291+190441 (L8 V) - This is the coolest L dwarf currently known, and it shows a possible lithium line at our detection limit (EW ≤ 9.4 Å). The spectrum is quite smooth throughout the far optical region and shows weak CrH and even weaker FeH bands. The only other obvious molecular absorption is H_2O near 9300 Å. Lines of the alkali metals are still present with Na I exceedingly weak, K I extremely broadened, and Rb I and Cs I very strong. The near-infrared spectrum (Figure 5) shows a distinct CO bandhead and strong absorption by H_2O.

• Gl 229B (T dwarf) - Located 7.″7 away from the M1 dwarf Gl 229A, this object was discovered by Nakajima et al. (1995). Like 2MASS J1632291+190441, this object shows strong Cs I lines and a strong H_2O band in Figure 7, but in Gl 229B the hydrides have completely disappeared. Despite similiarities in the far optical region, though, the K-band spectra (Figure 5) show pronounced differences, with 2MASS J1632291+190441 exhibiting weak CO bands and Gl 229B showing strong absorption by CH_4.

11. Appendix B: Notes on Other Objects

Several of the non-L-dwarf objects listed in Tables 1A and 2 are worthy of special mention. Twenty-two of these are ultra-cool M dwarfs (type M7 V or cooler). Distance estimates for these are listed in Table 13. Notes on individual objects of interest are given below:

• 2MASS J0149090+295613 (M9.5 V) - An inspection of the POSS-I and POSS-II plates of the region revealed that this is a high proper motion star with $\mu = 0.''51/\mathrm{yr}$ at $PA = 156°$. (As such, it does not strictly belong in the sample since it has a POSS-I E-plate counterpart — any non-motion object with identical magnitudes and colors would not have been chosen.) Despite its large motion, it was not detected by the proper motion surveys of Luyten (1979b, 1980) because it is within a few arcseconds of a brighter star at the epoch of the POSS-I survey and because it is invisible on the POSS-I O plate. Our first follow-up observations on 1997 Dec 07 (UT) showed an object with a rich, time-variable spectrum of very stong emission lines. In particular, the equivalent width (EW) of the Hα line was 300 Å. Subsequent observations of the object on 1997 Dec 24 (UT) from the Palomar 5m telescope along with additional Keck observations on 1998 Jan 22, 23, 24 (UT) showed an object with the spectrum of a "normal" M9.5 dwarf. In these quiescent spectra, only the Hα line is still seen in emission, and then at a mere ∼10 Å EW. Its estimated distance is 21 pc. See the companion paper by Liebert et al. (1998a) for more on this intriguing object.

• 2MASS J0244463+153531 (M5 V + M5.5 V) - This is a close (∼2″) double M dwarf.

• 2MASP J0348036+234411 (M7.5 V) - This is an ultra-cool M dwarf at an estimated distance of 46 pc. This object has been announced as a possible Pleiad brown dwarf and named "NOT 1" by Festin (1997, 1998) who, to make it consistent with Pleiades membership, suggests that the object is an equal-magnitude binary. We suggest, however, that it is merely a foreground object.

• 2MASS J0401096+182808 (carbon star) - This is a carbon star as identified by weak bands of CN throughout its far optical spectrum. It is an unusual carbon star, however, in that it shows *emission* lines

Fig. 1.— The $J - K_s$ vs. $R - K_s$ diagram for catalogued M dwarfs (mostly from Leggett 1992), 2MASS discoveries from this paper, the brown dwarf candidate GD 165B, and the methane brown dwarf Gl 229B. Approximate spectral types (see §5) are shown along the locus of points.

Fig. 2.— Finder charts for each of the 2MASS L dwarfs listed in Table 3. For each object, two views are shown — the POSS-I E (R-band) image on the left and the 2MASS K_s-band image on the right. Each view is to the same scale, five arcminutes on a side with north up and east to the left. The L dwarf is labelled with tick marks on the 2MASS image. Note that the 2MASS image does not always cover the full 5×5 arcminute field.

Fig. 3.— Spectra of all 26 dwarfs listed in Table 3. The flux scale is in units of F_λ normalized to one at 8250 Å. Integral offsets have been added to the flux scale to separate the spectra vertically. All spectra shown here were taken during our Keck follow-up runs except for the spectrum of GD 165B which is from Kirkpatrick et al. (1998) and Gl 229B which is from Oppenheimer et al. (1998).

Fig. 4.— Enlarged spectra of a late-M, early-to-mid-L, and late-L dwarf. Prominent features are marked. Note the absence of oxide absorption in the L dwarfs along with the dominance of alkali lines and hydride bands.

Fig. 5.— Near-infrared spectra of the two coolest 2MASS L dwarfs taken with CGS4 on UKIRT. Also shown for comparison is the Geballe et al. (1996) spectrum of the only known T-dwarf Gl 229B, also taken with CGS4 on UKIRT. The flux scale is in units of F_λ normalized to one at 2.20 μm. Integral offsets have been added to the flux scale to separate the spectra vertically. Note the absence of methane absorption and the continued presence of CO absorption in the late-L dwarfs.

Fig. 6.— The L-dwarf spectral sequence. This is a subset of the Keck LRIS data of Figure 3, but showing only one spectrum for each subclass from L0 through L8. Also shown for comparison is the Oppenheimer et al. spectrum of Gl 229B and three late-M dwarfs from Table 1A, also taken with LRIS on Keck.

Fig. 7.— Detailed portions of two wavelength regions from Figure 7. Each of these regions contains several diagnostics useful for spectral classification. Prominent lines and bands are marked. See §6.2 and Table 6 for a details.

Fig. 8.— Spectral ratios for the alkali lines, as defined in Table 7. The L dwarf primary standards along with the three M dwarfs from Figure 7 are shown by the large dots. The other L dwarfs ar shown as smaller dots, calculation of their final spectral types being described in §6.2.5.

Fig. 9.— Same as Figure 9 except showing the oxide ratios defined in Table 7.

Fig. 10.— Same as Figure 9 except showing the hydride ratios defined in Table 7.

Fig. 11.— Same as Figure 9 except showing the composite alkali/oxide ratios from Table 7.

Fig. 12.— Same as Figure 9 except showing the color ratios defined in Table 7.

Fig. 13.— (a) A plot of the 2MASS-measured J-K_s color vs. spectral class for the L dwarfs of Table 3 (open circles). Also shown for comparison are late-M dwarfs (filled circles) from Tinney et al. (1993) and Leggett (1992) along with Gl 229B (open star). From late-M through the L sequence there is a general trend of redder color with later spectral type, although the scatter at any given L class is on the order of ~0.3 mag. Note however the abrupt change in color caused by the onset of methane absorption at K_s in Gl 229B. (b) The same as for panel (a), except that the I magnitudes for the L dwarfs are measured directly off the LRIS spectra. Again, there is a monotonic trend (with some scatter) from late-M through the L sequence.

Fig. 14.— The $J-H$ vs. $H-K_s$ diagram for M and L dwarfs. The M dwarfs (filled circles) are from Leggett (1992) and the L dwarfs (open circles) are from this paper. The position of Gl 229B is shown by an open star. Tracks for dwarfs (solid line) and giants (dashed line) from Bessell & Brett (1988) are also shown.

Fig. 15.— Equivalent width measures for all 25 L dwarfs as tabulated in Table 9. (a) Hα emission strength; (b) Li I strength; (c) Rb I strength; (d) Cs I strength.

Fig. 16.— Detailed portions of the spectra near the Hα emission line for those objects with Hα detections

sample cooler than ~1400 K may not show lithium absorption either since lithium will have formed into LiCl. These argruments therefore suggest that the lithium test as performed on our spectra provides only a lower bound to the number of brown dwarfs contained in our sample. Based on the number which show lithium absorption, then, we can claim that *at least one third* off all known L dwarfs are substellar.

We can make other checks on the substellarity independent of the lithium test, too. Figure 18 shows the observational HR diagram for the L dwarfs and some late-M dwarfs with trigonometric parallax measures. Also plotted are theoretical models from Baraffe et al. (1998).[15] The models show that for an age of 1 Gyr, mid- to late-L dwarfs are all substellar; at much larger ages (10 Gyr), the earliest L dwarfs are stellar, with the later L dwarfs being comprised of transition objects and brown dwarfs. These results agree qualitatively with those from the lithium test.

Another check on substellarity can be made by comparing the effective temperatures of these objects (from the molecular equilibrium analysis of §8.2) to the predictions of model interiors. The effective temperature as a function of time is shown in Figure 19 for a variety of masses from 0.010 $M_\odot$ to 0.100 $M_\odot$. In the top panel of the figure is shown the latest models of Burrows et al. (1997), and in the bottom panel those of Baraffe et al. (1998). Indicated by the thick horizontal lines on each panel is the approximate temperature range spanned by L dwarfs. According to the Burrows et al. models, the lowest mass stars (~0.078 $M_\odot$) eventually stabilize at a temperature near 1750 K (shown by the dashed line). This dividing line lands squarely in the middle of the L dwarf temperature range, meaning that the latest L dwarfs are all substellar and the earlier ones represent a mixture of stars and brown dwarfs. Note that brown dwarfs can exist at the earliest L types with ages as old as 2 Gyr. According to the Baraffe et al models, the lowest mass stars (~0.075 $M_\odot$) stabilize at temperatures near 2000 K, meaning that the entire L sequence is "sub"stellar. However, objects with masses between 0.072 and 0.075 $M_\odot$ may stabilize after more than a Hubble time at a temperature near 1700 K. In this case, the latest L dwarfs are all brown dwarfs with earlier types representing a mixture of brown dwarfs and "transition objects".

All checks therefore agree that a substantial fraction of L dwarfs are brown dwarfs. Atmospheric modelling which includes the effects of grain depletion and grain opacities is now being developed, and once it accurately reproduces colors and observed spectra of L dwarfs, we will have a much better understanding of the exact makeup of the L dwarf classes. Another excellent diagnostic can be obtained for close binary systems with one or more L dwarf components – here, dynamical masses can be determined and used as additional checks against the theory. In this regard, closer scrutiny of the L dwarfs so far discovered is certainly warranted.

8.4. Luminosity and Mass Functions for L Dwarfs

Using the statistics quoted in §3 along with the absolute magnitudes given in Table 10, we can obtain a preliminary luminosity function (LF) for L dwarfs. Converting this LF into a mass function (MF) is a very difficult undertaking because any given L type represents a range of masses at different ages. Observationally, we cannot obtain either the mass of the age for an isolated L dwarf, so the computation must involve our observational statistics on Li detections (to assign an age spread) and theoretical isochrones (to assign mass spreads). In fact, for the L dwarfs which are substellar, the L spectral sequence represents an evolutionary sequence where the objects cool to later L (and T) types with advancing age.

These computations are complex and beyond the scope of this paper. Please refer to the companion paper by Reid et al. (1998) for a full discussion on our derived LF and MF.

9. Conclusions

Using 371 sq. deg. of 2MASS data, we have obtained spectroscopic classifications of 51 objects with no optical counterparts. A large fraction of these were found to be dwarfs cooler than the coolest known M dwarf with spectra lacking the familiar oxide bands of M stars. We have placed these new objects into a new spectral class called "L". We have presented criteria defining this new class and have established a recipe for the spectral classification of other L dwarfs using a grid of objects set aside as spectral standards. We have shown that several of the L dwarfs known show Li I absorption, indicating that at least one third of

[15] These models do not yet incorporate grains and fail to predict the red $J-K_s$ colors seen for L dwarfs. As a result, models are overplotted only for the $I-K_s$ diagrams, where the agreement is reasonable.

Delfosse, X., Tinney, C. G., Forveille, T., Epchtein, N., Bertin, E., Borsenberger, J., Copet, E., de Batz, B., Fouque, P., Kimeswenger, S., LeBertre, T., Lacombe, F., Rouan, D., & Tiphene, D. 1997, A&A, 327, L25.

Festin, L. 1997, A&A, 322, 455.

Festin, L. 1998, A&A, 333, 497.

Geballe, T. R., Kulkarni, S. R., Woodward, C. E., & Sloan, G. C. 1996, ApJL, 467, 101.

Gliese, W., & Jahreiss, H. 1991, Preliminary Version of the Third Catalog of Nearby Stars, ADC CD-ROM, Vol. 1, No. 1.

Golimowski, D. A., Burrows, C. J., Kulkarni, S. R., Oppenheimer, B. R., & Brukardt, R. A. 1998, AJ, 115, 2579.

Gordon, C. P. 1971, PASP, 83, 667.

Hamuy, M., Suntzeff, N. B., Heathcote, S. R., Walker, A. R., Gigoux, P., & Phillips, M. M. 1994, PASP, 106, 566.

Jones, H. R. A., & Tsuji, T. 1997, ApJ, 480, L39.

Keenan, P. C., & Morgan, W. W. 1941, ApJ, 94, 501.

Kirkpatrick, J. D. 1994, in The Bottom of the Main Sequence — And Beyond, ed. C. G. Tinney (Springer-Verlag: Heidelberg), p. 140

Kirkpatrick, J. D. 1998, in Brown Dwarfs and Extrasolar Planets, ed. R. Rebolo, E. Martín, and M. R. Zapatero-Osorio (ASP: San Francisco), p. 405

Kirkpatrick, J. D., Allard, F., Bida, T., Zuckerman, B., Becklin, E. E., Chabrier, G., & Baraffe, I. 1998, ApJ, submitted.

Kirkpatrick, J. D., Beichman, C. A., & Skrutskie, M. F. 1997a, ApJ, 476, 311.

Kirkpatrick, J. D., Henry, T. J., & Irwin, M. J. 1997b, AJ, 113, 1421.

Kirkpatrick, J. D., Henry, T. J., & Liebert, J. 1993, ApJ, 406, 701.

Kirkpatrick, J. D., Henry, T. J., & McCarthy, D. W., Jr. 1991, ApJS, 77, 417.

Kirkpatrick, J. D., Henry, T. J., & Simons, D. A. 1995, AJ, 109, 797.

Leggett, S. K. 1992, ApJS, 82, 351.

Liebert, J., Kirkpatrick, J. D., Reid, I. N., & Fisher, M. D. 1998a, ApJ, in prep.

Liebert, J., et al. 1998b, in prep.

Luyten, W. J. 1979a, LHS Catalogue (University of Minnesota, Minneapolis).

Luyten, W. J. 1979b, NLTT Catalogue, Vol. I-II (University of Minnesota, Minneapolis).

Luyten, W. J. 1980, NLTT Catalogue, Vol. III-IV (University of Minnesota, Minneapolis).

Martín, E. L, Basri, G., Delfosse, X., & Forveille, T. 1997, A&A, 327, L29.

Monet, D. G., Dahn, C. C., Vrba, F. J., Harris, H. C., Pier, J. R., Luginbuhl, C. B., & Ables, H. D. 1992, AJ, 103, 638.

Morgan, W. W., Keenan, P. C., & Kellman, E. 1943, An Atlas of Stellar Spectra, with an Outline of Spectral Classification (University of Chicago, Chicago).

Nakajima, T., Oppenheimer, B. R., Kulkarni, S. R., Golimowski, D. A., Matthews, K., & Durrance, S. T. 1995, Nature, 378, 463.

Nelson, B. et al. 1998, in prep.

Oke, J. B., Cohen, J, G, Carr., M., Cromer, J., Dingizian, A., Harris, F. H., Labrecque, S., Lucinio, R., Schaal, W., Epps, H., & Miller, J 1995, PASP, 107, 375.

Oppenheimer, B. R., Kulkarni, S. R., Matthews, K., & van Kerkwijk, M. H. 1998, ApJ, 502, 932.

Persson, S. E., Murphy, D. C., Krzeminski, W., Roth, M., & Reike, M. J. 1998, AJ, 116, 2475.

Pickering, E. C. 1890, Harvard College Obs. Ann., 27, 1.

Pickering, E. C. 1908, Harvard Obs. Circ., 145.

Reid, I. N. et al. 1998, in preparation.

Ruiz, M. T., Leggett, S. K., & Allard, F., 1997, ApJ, 491, L107.

Secchi, A. 1866, Comptes Rendus, 63, 621.

TABLE 1A

OBJECTS MEETING SEARCH CRITERIA IN 371 SQ. DEG. (SUBSAMPLE WITH $J - K_s \geq 1.30$)

Object Name (1)	l^{II} (2)	b^{II} (3)	$(K_s)_{ins}$ (4)	$(J-K_s)_{ins}$ (5)	Obs. Date (UT) (6)	Exp. (s) (7)	Spectral Type (8)
2MASS J0010037+343610	111.3	-27.1	14.18	1.30	1997 Dec 09	1200	M8 V
2MASS J0030438+313932	117.8	-31.0	13.82	1.43	1998 Jan 22	1200	(see Table 3)
2MASS J0055384+275652	124.1	-34.9	14.20	1.39	1997 Dec 08	1200	M7 V
2MASS J0129122+351758	131.6	-26.9	14.48	2.00	1998 Jan 23	3600	(see Table 3)
					1998 Jan 24	3600	
2MASS J0147334+345311	135.8	-26.6	14.46	1.38	1997 Nov 09	2400	(see Table 3)
2MASS J0149090+295613	137.6	-31.3	11.82	1.40	1997 Dec 07	2100	M9.5 V[a]
					1997 Dec 24	2400	
					1998 Jan 22	1200	
					1998 Jan 23	1200	
					1998 Jan 24	1200	
2MASS J0242435+160739	158.2	-39.0	14.06	1.48	1998 Jan 24	2400	(see Table 3)
2MASS J0245147+120350	161.8	-42.1	13.99	1.35	1997 Nov 09	900	M5 V
2MASS J0251222+252124	154.4	-30.1	14.20	1.36	1998 Jan 23	1200	M9 V
2MASS J0251254+262504	153.7	-29.2	14.30	1.40	1998 Jan 23	1200	M9 V
2MASS J0326137+295015	158.7	-22.1	13.62	1.61	1998 Jan 24	1500	(see Table 3)
2MASS J0326342+300012	158.7	-21.9	13.80	1.38	1998 Jan 24	300	reddened bkg star[b]
2MASS J0327091+300130	158.8	-21.8	14.35	2.41	1998 Jan 22	1200	reddened bkg star[b]
2MASS J0327205+294959	159.0	-21.9	13.82	1.85	1998 Jan 23	1200	reddened bkg star[b]
2MASS J0327210+295816	158.9	-21.8	14.12	1.38	1998 Jan 24	300	reddened bkg star[b]
2MASS J0327235+295230	158.9	-21.9	12.90	1.94	1998 Jan 22	1200	reddened bkg star[b]
2MASS J0327304+295558	158.9	-21.8	14.13	1.78	1998 Jan 24	300	reddened bkg star[b]
2MASS J0327364+294118	159.1	-22.0	13.98	1.31	1998 Jan 24	300	reddened bkg star[b]
2MASS J0328072+290424	159.6	-22.4	14.05	1.38	1998 Jan 24	300	reddened bkg star[b]
2MASS J0328543+293827	159.4	-21.9	14.40	1.43	1998 Jan 24	300	reddened bkg star[b]
2MASS J0329202+291734	159.7	-22.1	14.48	1.36	1998 Jan 24	300	reddened bkg star[b]
2MASS J0329214+290533	159.8	-22.2	13.79	1.49	1998 Jan 24	300	reddened bkg star[b]
2MASS J0329267+300057	159.2	-21.5	14.38	1.71	1998 Jan 24	300	reddened bkg star[b]
2MASS J0355419+225702	169.0	-23.0	14.05	1.91	1997 Dec 07	900	(see Table 3)
					1997 Dec 08	1200	
					1998 Jan 24	1200	
2MASS J0401096+182808	173.5	-25.3	9.10	4.68	1997 Dec 08	600	carbon star[c]
					1997 Dec 24	2400	
2MASS J0724096+162302	201.7	14.5	14.40	1.31	1997 Dec 09	1200	M5.5 V
2MASS J0850359+105716	216.5	31.4	14.27	1.94	1997 Nov 09	2400	(see Table 3)
					1997 Dec 07	1200	
					1997 Dec 08	1200	
					1997 Dec 09	1200	
					1998 Jan 24	4800	
2MASS J0857258+172052	210.3	35.4	10.49	4.30	1998 Jan 22	1200	carbon star[c,d]
2MASS J0913032+184150	210.3	39.4	14.00	1.68	1998 Jan 22	2400	(see Table 3)
2MASS J0914188+223813	205.6	40.9	13.68	1.38	1998 Jan 23	1200	M9.5 V
2MASS J0918382+213406	207.3	41.6	13.68	1.72	1998 Jan 22	3600	(see Table 3)
2MASS J0921457+191812	210.5	41.5	14.34	2.16	1998 Jan 22	2161	QSO[e]
2MASS J1145572+231730	223.8	74.7	13.65	1.67	1997 Dec 07	1200	(see Table 3)
2MASS J1146345+223053	226.8	74.6	12.44	1.59	1997 Dec 07	1200	(see Table 3)
2MASS J1155009+230706	227.3	76.6	14.12	1.60	1998 Jan 22	2400	(see Table 3)

TABLE 1B

OBJECTS MEETING SEARCH CRITERIA IN 371 SQ. DEG. (SUBSAMPLE WITH $J - K_s \leq 0.40$)

Object Name (1)	λ (2)	β (3)	$(K_s)_{ins}$ (4)	$(J-K_s)_{ins}$ (5)	Identification (6)	Obs. Date (UT) (7)
2MASS J0031007+332004	21.3	27.3	12.99	0.39	asteroid (1235) Schorria	1997 Nov 15
2MASS J0242258+294101	47.3	13.3	12.64	0.31	asteroid 1981 YA1	1997 Nov 16
2MASS J0244401+244224	46.3	8.4	13.06	0.38	asteroid 1993 XO	1997 Nov 16
2MASS J0251318+284917	49.0	11.8	13.37	0.35	asteroid (3139) Shantou	1997 Nov 16
2MASS J0251447+252347	48.0	8.6	12.45	0.27	asteroid (1066) Lobelia	1997 Nov 16
2MASS J0254141+275547	49.3	10.8	13.22	0.32	asteroid (3300) McGlasson	1997 Nov 16
2MASS J0849065+091520	132.1	-8.2	14.35	0.32	asteroid (837) Schwarzschilda	1997 Nov 16
2MASS J0850138+061125	133.2	-11.1	12.11	0.31	asteroid (136) Austria	1997 Nov 16
2MASS J0850274+073719	132.9	-9.7	9.04	0.39	motion star LHS 2056	1997 Nov 16
2MASS J0851360+174933	130.4	0.2	12.00	0.30	asteroid (556) Phyllis	1997 Nov 15
2MASS J0852144+161547	131.0	-1.3	14.35	0.28	asteroid (2320) Blarney	1997 Nov 15
2MASS J0915347+212728	134.8	5.3	13.57	0.38	asteroid (2766) Leeuwenhoek	1998 Jan 12
2MASS J0916286+231038	134.4	7.0	13.97	0.39	asteroid (4041) Miyamotoyohko	1998 Jan 12
2MASS J0924386+152849	138.6	0.3	11.93	0.39	asteroid (569) Misa	1997 Nov 24
2MASS J2251228+293944	357.4	33.8	13.73	0.31	motion star LHS 529	1997 Nov 15

TABLE 3

THE TWENTY-FIVE "L" DWARFS AND GL 229B

Object Name (1)	Spectral Type (2)	K_s (3)	$J-K_s$ (4)	$H-K_s$ (5)	I_{spec} (6)	$I_{spec}-K_s$ (7)	dist. (pc) (8)
2MASP J0345432+254023	L0 V	12.70±0.04	1.33±0.05	0.53±0.05	16.98	4.28	28.2*
2MASS J0147334+345311	L0.5 V	13.59±0.04	1.35±0.06	0.57±0.07	18.07	4.48	*32*
2MASS J1439284+192915	L1 V	11.58±0.04	1.18±0.06	0.47±0.06	16.02	4.44	15.1*
2MASS J1439409+182637	L1 V	14.53±0.11	1.68±0.15	0.94±0.17	19.87	5.34	*50*
2MASS J1145572+231730	L1.5 V	13.87±0.08	1.64±0.10	0.57±0.10	18.62	4.75	*35*
2MASS J0242435+160739	L1.5 V	14.26±0.08	1.41±0.10	0.56±0.10	19.01	4.75	*44*
2MASS J1334062+194034	L1.5 V	13.99±0.06	1.55±0.09	0.84±0.09	18.76	4.77	*38*
Kelu-1	L2 V	11.81±0.03	1.57±0.04	0.60±0.04	16.51	4.70	*10**
2MASS J0030438+313932	L2 V	13.99±0.06	1.50±0.08	0.59±0.08	18.82	4.83	*35*
2MASS J1342236+175156	L2.5 V	14.59±0.11	1.47±0.14	0.53±0.13	19.81	5.22	*45*
2MASS J0918382+213406	L2.5 V	14.21±0.07	1.45±0.10	0.43±0.09	18.68	4.47	*30*
2MASS J1146345+223053	L3 V	12.63±0.04	1.60±0.06	0.61±0.08	17.62	4.99	*18**
DENIS-P J1058.7−1548	L3 V	12.53±0.03	1.65±0.04	0.69±0.04	17.64	5.11	*23**
2MASS J0913032+184150	L3 V	14.20±0.05	1.72±0.09	0.64±0.08	19.07	4.87	*35*
2MASS J0355419+225702	L3 V	14.25±0.07	1.85±0.11	0.78±0.10	19.49	5.24	*35*
2MASS J0326137+295015	L3.5 V	13.83±0.06	1.60±0.08	0.55±0.08	19.17	5.34	*27*
2MASS J0129122+351758	L4 V	14.68±0.09	2.06±0.18	0.61±0.13	19.43	4.75	*39*
2MASS J1155009+230706	L4 V	14.30±0.12	1.68±0.15	0.48±0.15	19.30	5.00	*33*
GD 165B	L4 V	*14.15*	*1.58*		19.57	5.42	31.5
2MASS J1328550+211449	L5 V	14.25±0.10	1.79±0.15	0.63±0.13	20.07	5.82	*30**
DENIS-P J1228.2−1547	L5 V	12.81±0.03	1.57±0.05	0.56±0.05	18.05	5.24	*17**
2MASS J1553214+210907	L5.5 V	14.68±0.12	2.00±0.21	0.66±0.19	20.79	6.11	*34*
2MASS J0850359+105716	L6 V	14.46±0.07	1.99±0.14	0.76±0.12	20.33	5.87	*41**
DENIS-P J0205.4−1159	L7 V	12.99±0.04	1.56±0.05	0.60±0.05	18.28	5.29	16.6*
2MASS J1632291+190441	L8 V	13.98±0.05	1.88±0.09	0.61±0.07	19.98	6.00	*20**
Gl 229B	T dwarf	14.3	-0.1	0.0	19.53	5.23	5.8

NOTE.—The photometry reported here is calibrated photometry, not instrumental values like those listed in Tables 1A and 2. Please note that both the positional name and the calibrated photometry for the 2MASS objects may undergo slight revisions at a later date when the catalogs covering these scans are distributed to the community. Also note that the tabulated magnitude for GD 165B is K, not K_s. Italics in column 8 refers to a distance estimated from the near-infrared magnitudes and spectral type of the object; those not in italics are measured via trigonometric parallax. As asterisk (*) in this column indicates an object on the USNO parallax program.

TABLE 5

SUMMARY OF LETTERS TO GUIDE CHOICE OF NEW SPECTRAL TYPE

Letter (1)	Status (2)	Notes (3)
A	in use	standard spectral class
B	in use	standard spectral class
C	in use	standard carbon star class
D	ambiguous	confusion with white dwarf classes DA, DB, DC, etc.
E	ambiguous	confusion with elliptical galaxy morphological types E0-E7
F	in use	standard spectral class
G	in use	standard spectral class
H	ok	—
I	problematic	transcription problems with I0 (10, Io) and I1 (11, II, Il)
J	in use	standard carbon star class
K	in use	standard spectral class
L	ok	—
M	in use	standard spectral class
N	in use	standard carbon star class
O	in use	standard spectral class
P	problematic?	incorrect association with Planets?
Q	problematic?	incorrect association with QSOs?
R	in use	standard carbon star class
S	in use	standard carbon star class
T	ok	—
U	problematic?	incorrect association with Ultraviolet sources?
V	problematic	confusion with vanadium oxide (V0 vs. VO)
W	ambiguous	confusion with Wolf-Rayet WN and WR classes
X	problematic	incorrect association with X-ray sources
Y	ok	—
Z	problematic?	incorrect implication that we've reached "the end"?

TABLE 6—*Continued*

Subclass (1)	Spectral Characteristics[a] (2)	Example (3)
L7	TiO 8432 Å virtually gone FeH 8692, 9896 Å and CrH 8611 Å still weakening with CrH 8611 Å still deeper than FeH 8692 Å K I even broader Rb I and Cs I still strengthening Na I still weakening	DENIS-P J0205.4−1159
L8	FeH 8692, 9896 Å very weak CrH 8611 Å still weakening though still stronger than FeH 8692 Å K I even broader Rb I and Cs I still strengthening Na I barely perceptible	2MASS J1632291+190441

[a]Relative depths of bands refer to spectra with absolute flux calibration (F_λ) like those in Fig. 7 and 8.

TABLE 8A

VALUES OF SPECTRAL DIAGNOSTICS FOR THE SPECTRA IN FIGURE 7

Object Name (1)	Type (2)	CrH-a (3)	Rb-b/TiO-b (4)	Cs-a/VO-b (5)	Color-d (6)
2MASS J1214063+202702	M7 V	0.996	0.649	0.867	2.793
2MASS J1434264+194050	M8 V	1.034	0.588	0.795	3.725
2MASS J1239194+202952	M9 V	1.043	0.576	0.736	5.345
2MASP J0345432+254023	L0 V	1.161	0.662	0.781	6.654
2MASS J1439284+192915	L1 V	1.371	0.812	0.856	7.333
Kelu-1	L2 V	1.537	1.048	1.029	6.700
2MASS J1146345+223053	L3 V	1.636	1.155	1.125	7.210
2MASS J1155009+230706	L4 V	1.909	1.323	1.258	9.713
DENIS-P J1228.2−1547	L5 V	2.203	1.658	1.488	14.406
2MASS J0850359+105716	L6 V	1.786	1.703	1.561	15.549
DENIS-P J0205.4−1159	L7 V	1.551	2.189	1.604	22.027
2MASS J1632291+190441	L8 V	1.289	2.564	1.626	30.015

TABLE 9

EQUIVALENT WIDTH MEASUREMENTS FOR THE DWARFS IN TABLE 3

Object Name (1)	Spectral Type (2)	Hα emis. 6563 Å EW (Å) (3)	Li I abs. 6708 Å EW (Å) (4)	Rb I abs. 7948 Å EW (Å) (5)	Cs I abs. 8521 Å EW (Å) (6)
2MASP J0345432+254023	L0 V	≤0.3	<0.5	2.7	1.5
2MASS J0147334+345311	L0.5 V	<0.5	<1.0	2.7	1.8
2MASS J1439284+192915	L1 V	<0.3	<0.3	3.2	1.8
2MASS J1439409+182637	L1 V	<0.6	5.6	3.5	2.0
2MASS J1145572+231730	L1.5 V	4.2	<0.4	3.5	2.1
2MASS J0242435+160739	L1.5 V	<0.5	<0.7	2.9	2.1
2MASS J1334062+194034	L1.5 V	4.2	<1.5	2.8	3.1
Kelu-1	L2 V	1.9	1.7	2.8	2.0
2MASS J0030438+313932	L2 V	4.4	<1.0	2.9	2.3
2MASS J1342236+175156	L2.5 V	<2.2	≤3.9	3.3:	1.8
2MASS J0918382+213406	L2.5 V	<0.3	<0.3	3.2	2.2
2MASS J1146345+223053	L3 V	≤0.3	5.1	3.7	2.4
DENIS-P J1058.7−1548	L3 V	1.6	<0.3	3.4	2.8
2MASS J0913032+184150	L3 V	<0.8	<1.0	3.2	2.2
2MASS J0355419+225702	L3 V	<0.5	<1.3	3.0:	2.6:
2MASS J0326137+295015	L3.5 V	9.1	<1.0	4.0	3.1
2MASS J0129122+351758	L4 V	<0.5	3.3	4.4	3.6
2MASS J1155009+230706	L4 V	<1.0	<0.5	4.6	3.1
GD 165B	L4 V	<0.8	<0.7	4.6	3.1
2MASS J1328550+211449	L5 V	<2.0	<3.0	6.6:	3.8
DENIS-P J1228.2−1547	L5 V	≤0.6	3.1	5.5	4.4
2MASS J1553214+210907	L5.5 V	<4.3	18.5	8.1:	5.0
2MASS J0850359+105716	L6 V	<0.9	15.2	4.9	4.7
DENIS-P J0205.4−1159	L7 V	<2.7	<1.3	6.8	5.7
2MASS J1632291+190441	L8 V	≤4.0	≤9.4	6.9	5.6
Gl 229B	T dwarf	...	...	...	5.9

NOTE.—Equivalent widths (EW) have typical errors of ±0.2 Å for most of the spectra presented here, but those with poorer signal-to-noise have errors of around ±0.5 Å.

TABLE 11

SPECTRAL FEATURES USABLE AS L DWARF TEMPERATURE INDICATORS

Atom or Molecule (1)	Observed Maxmimum (2)	Observed Disappearance (3)	Theoretical Explanation[a] (4)	Predicted Disappearance[a] (5)
TiO	~M8	~L2[b]	condenses into $CaTiO_3$	2300-2000 K
VO	~M9	~L4	depletes into solid VO	1700-1900 K
Na I	~M8?	~L8	forms into NaCl	~1150 K
FeH	~L4	>L8	... [c]	... [c]
CrH	~L5	>L8	converts into metallic CrH	~1400 K
Li I	~L6?	~L7?	forms into LiCl	≤1400 K
CO	...	...	C becomes bound to CH_4	1200-1500 K
Rb I	≥L8	...	forms into RbCl	≤1200 K
Cs I	≥L8	...	forms into CsCl	≤1200 K
K I	...	...	forms into KCl	≤1200 K
H_2O	...	...	disappears into H_2O condensate	~350 K

[a]Taken from Burrows & Sharp 1998.

[b]True for all bands except the one at 8432 Å which doesn't disappear until about L5-6.

[c]Not included in Burrows & Sharp 1998.

2MASS J0030438+313932

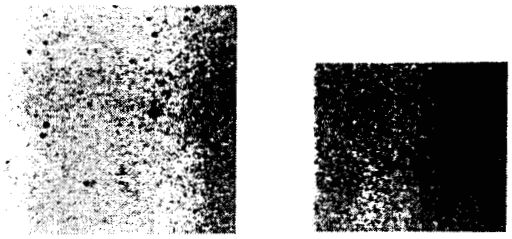

2MASP J0345432+254023

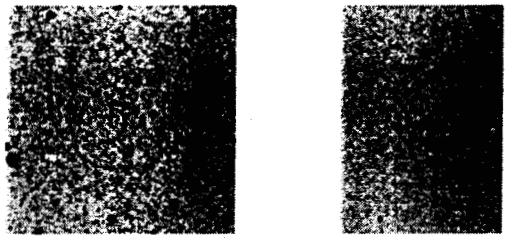

2MASS J0129122+351758

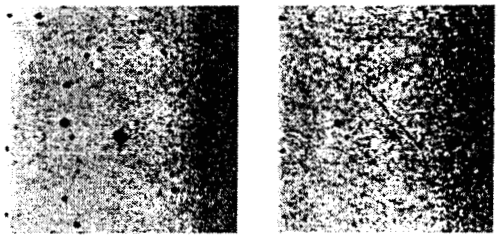

2MASS J0355419+225702

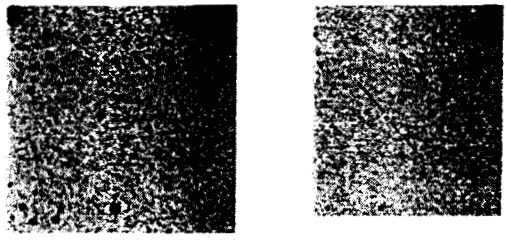

2MASS J0147334+345311

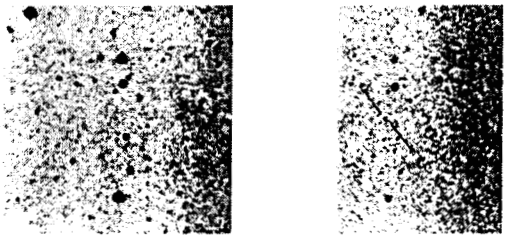

2MASS J0850359+105716

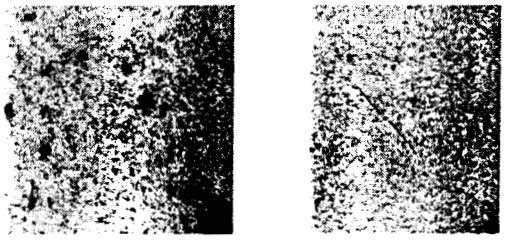

2MASS J0242435+160739

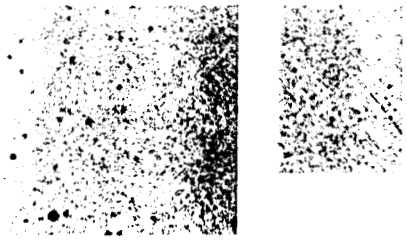

2MASS J0913032+184150

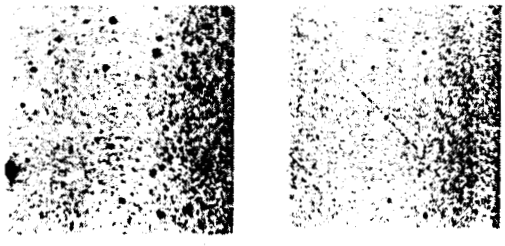

2MASS J0326137+295015

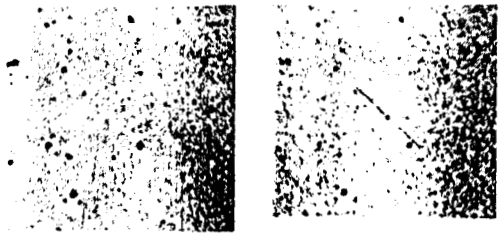

2MASS J0918382+213406

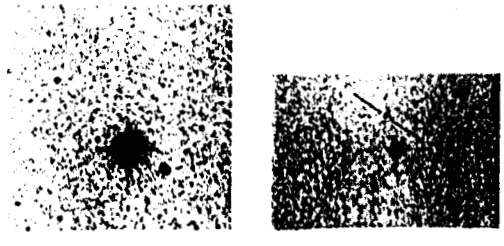

FIG. 2a

TABLE 13

ULTRA-COOL M DWARFS FROM TABLES 1A AND 2

Object Name (1)	Spectral Type (2)	J (3)	H (4)	K_s (5)	Estimated Dist. (pc) (6)
2MASS J0010037+343610	M8 V	15.66±0.07	15.08±0.09	14.38±0.07	82
2MASS J0055384+275652	M7 V	15.73±0.07	14.86±0.07	14.46±0.08	94
2MASP J0147362+365855	M7 V	14.8±0.1	14.2±0.1	13.6±0.1	65
2MASS J0149090+295613	M9.5 V	13.42±0.03	12.57±0.04	12.00±0.03	21
2MASS J0251222+252124	M9 V	15.89±0.07	14.97±0.07	14.40±0.07	67
2MASS J0251254+262504	M9 V	16.00±0.08	15.22±0.09	14.51±0.07	73
2MASP J0348036+234411	M7.5 V	14.27±0.04	13.64±0.05	13.23±0.04	46
2MASS J0914188+223813	M9.5 V	15.30±0.05	14.40±0.05	13.90±0.04	51
2MASS J1214063+202702	M7 V	15.67±0.07	15.08±0.08	14.45±0.11	97
2MASS J1239194+202952	M9 V	14.48±0.04	13.65±0.04	13.16±0.04	36
2MASS J1434264+194050	M8 V	15.55±0.06	14.83±0.09	14.39±0.11	76
2MASS J1710255+210715	M8 V	15.87±0.08	15.02±0.09	14.46±0.11	85
2MASS J2258066+154416	M7.5 V	16.18±0.09	15.35±0.11	14.71±0.12	107
2MASS J2258590+152047	M7 V	15.59±0.06	15.02±0.07	14.59±0.10	94
2MASS J2309462+154905	M8.5 V	15.01±0.06	14.34±0.06	13.91±0.07	53

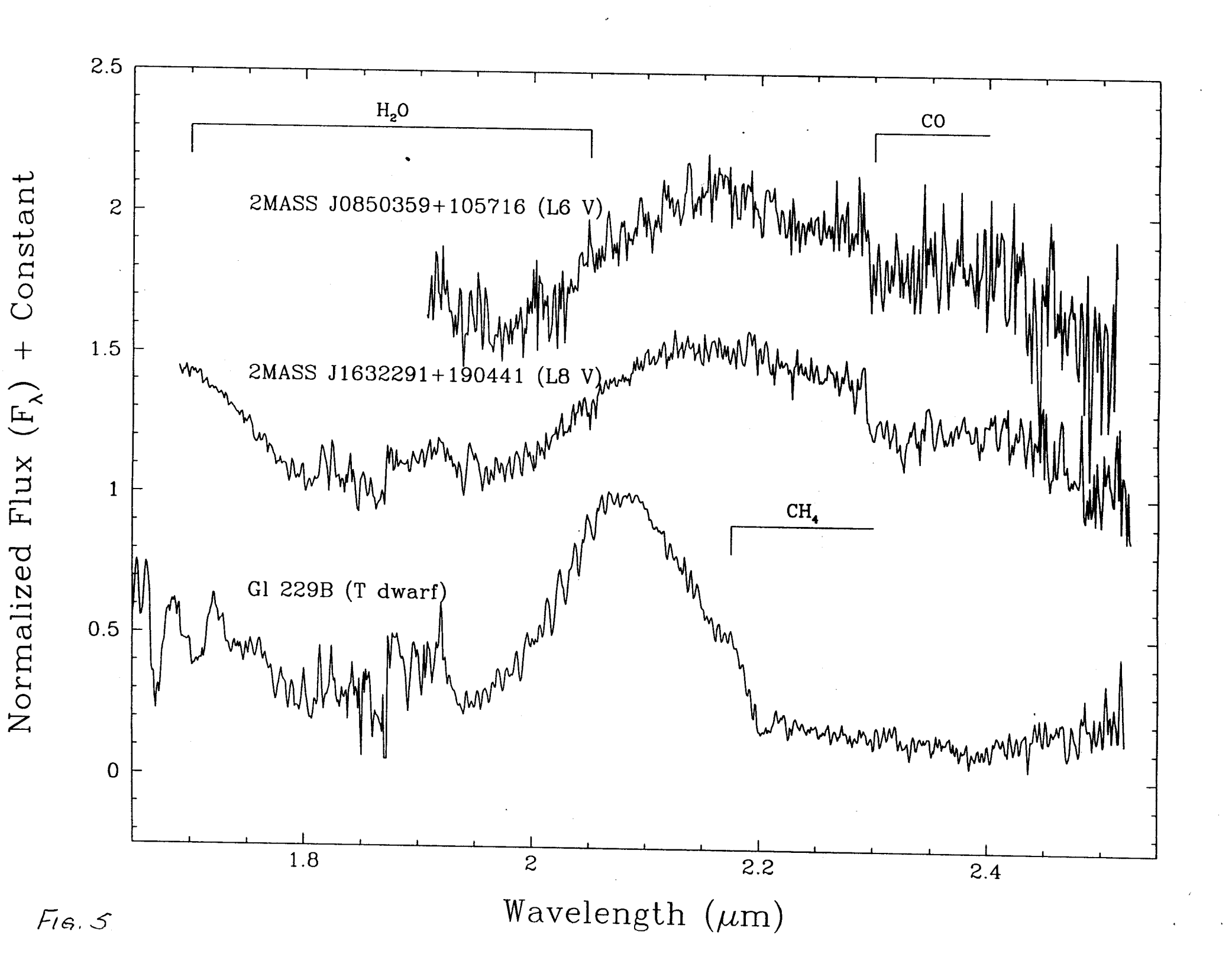
2.5
2
1.5
1
0.5
0
1.8
2
2.2
2.4
H2O
CO
CH4
2MASS J0850359+105716 (L6 V)
2MASS J1632291+190441 (L8 V)
Gl 229B (T dwarf)
Normalized Flux (Fλ) + Constant
Wavelength (μm)

FIG. 5

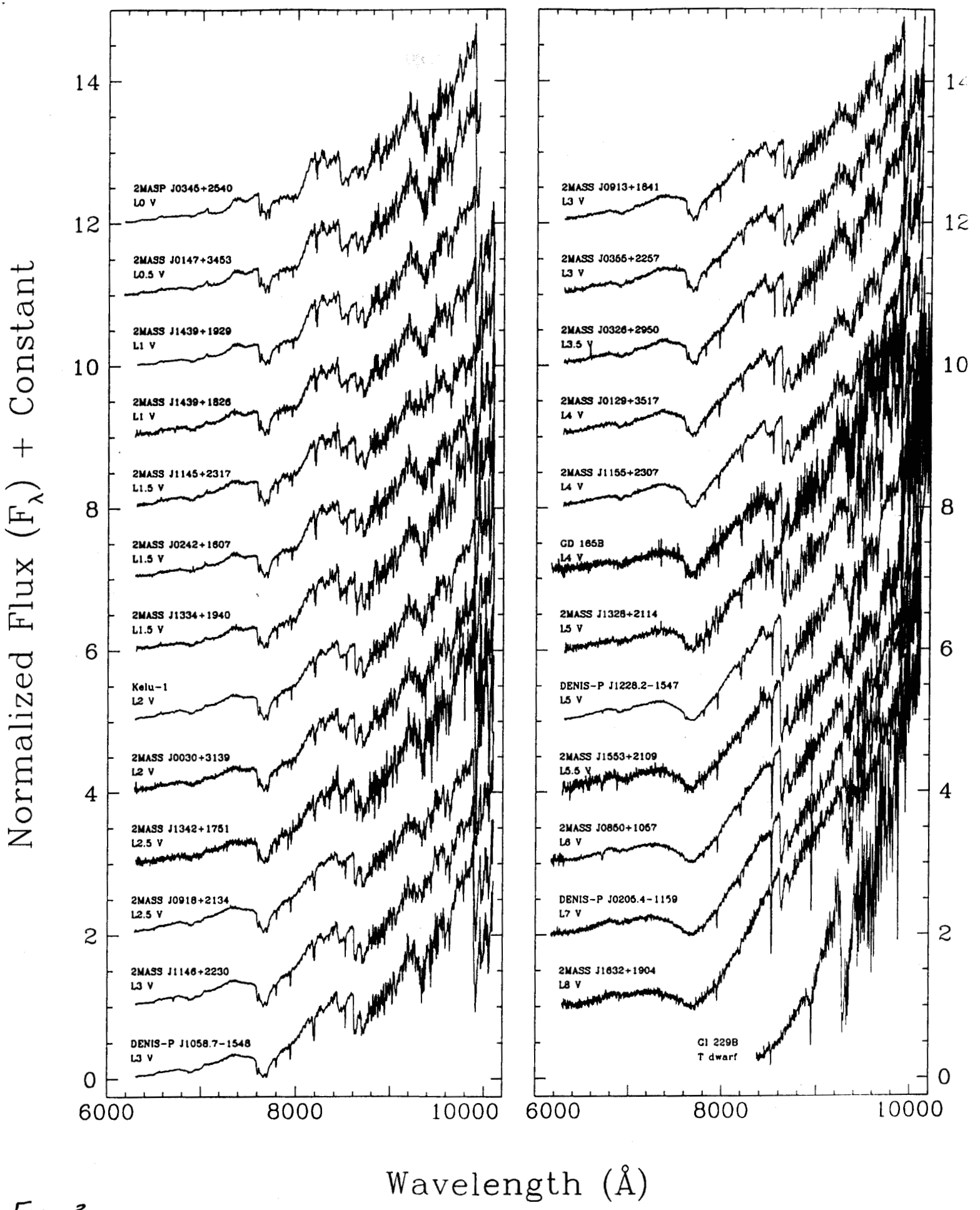
Normalized Flux (F_λ) + Constant
Wavelength (Å)
2MASP J0345+2540
L0 V
2MASS J0147+3453
L0.5 V
2MASS J1439+1929
L1 V
2MASS J1439+1826
L1 V
2MASS J1145+2317
L1.5 V
2MASS J0242+1607
L1.5 V
2MASS J1334+1940
L1.5 V
Kelu-1
L2 V
2MASS J0030+3139
L2 V
2MASS J1342+1751
L2.5 V
2MASS J0918+2134
L2.5 V
2MASS J1146+2230
L3 V
DENIS-P J1058.7-1548
L3 V
2MASS J0913+1641
L3 V
2MASS J0355+2257
L3 V
2MASS J0326+2950
L3.5 V
2MASS J0129+3517
L4 V
2MASS J1155+2307
L4 V
GD 165B
L4 V
2MASS J1328+2114
L5 V
DENIS-P J1228.2-1547
L5 V
2MASS J1553+2109
L5.5 V
2MASS J0850+1057
L6 V
DENIS-P J0205.4-1159
L7 V
2MASS J1632+1904
L8 V
Gl 229B
T dwarf
0
2
4
6
8
10
12
14
6000
8000
10000

Fig. 3.

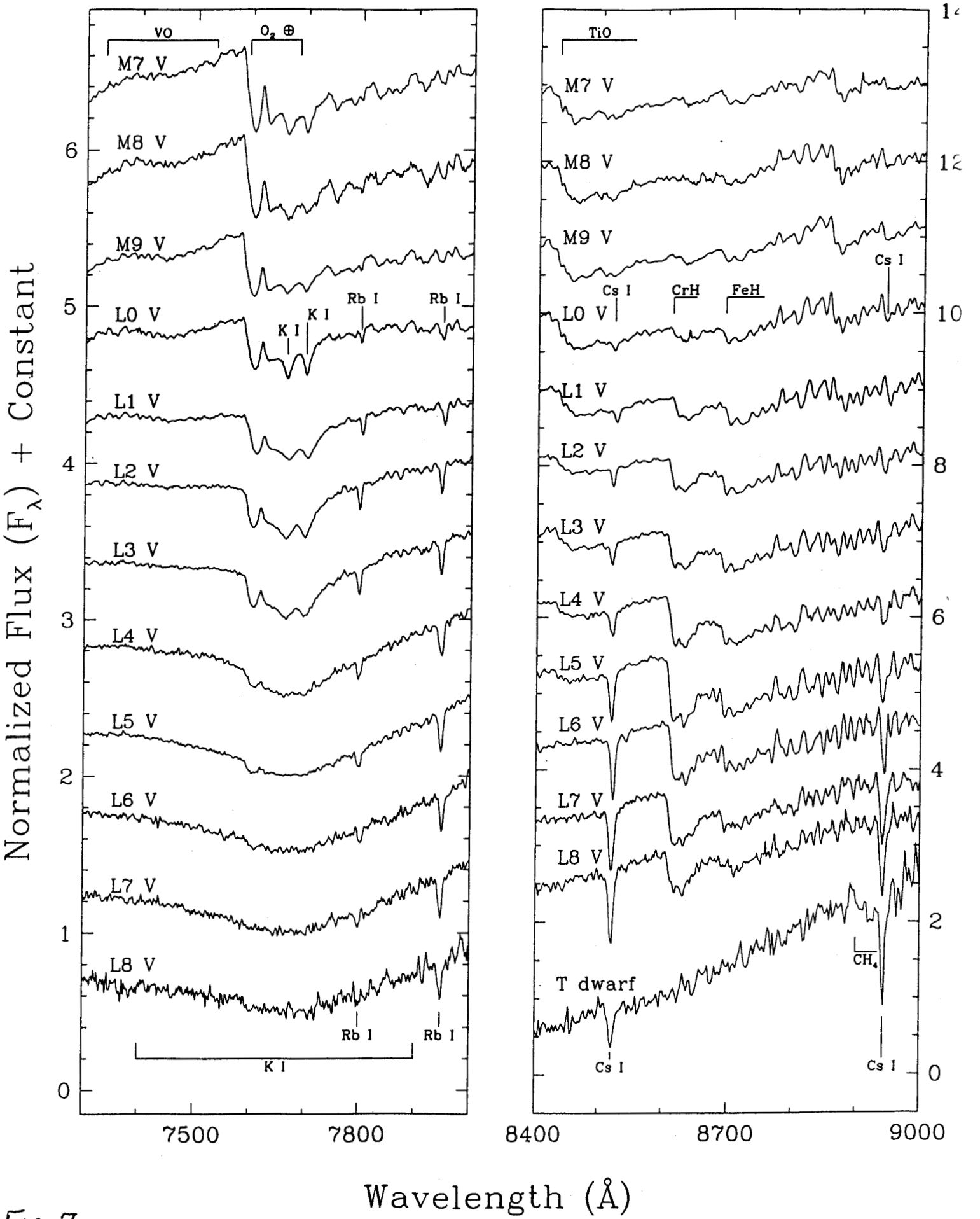
VO
O_2 ⊕
M7 V
M8 V
M9 V
L0 V
L1 V
L2 V
L3 V
L4 V
L5 V
L6 V
L7 V
L8 V
T dwarf
K I
K I
Rb I
Rb I
Rb I
Rb I
K I
TiO
Cs I
CrH
FeH
Cs I
CH_4
Cs I
Cs I
Normalized Flux (F_λ) + Constant
Wavelength (Å)
0
1
2
3
4
5
6
7500
7800
8400
8700
9000

FIG. 7.

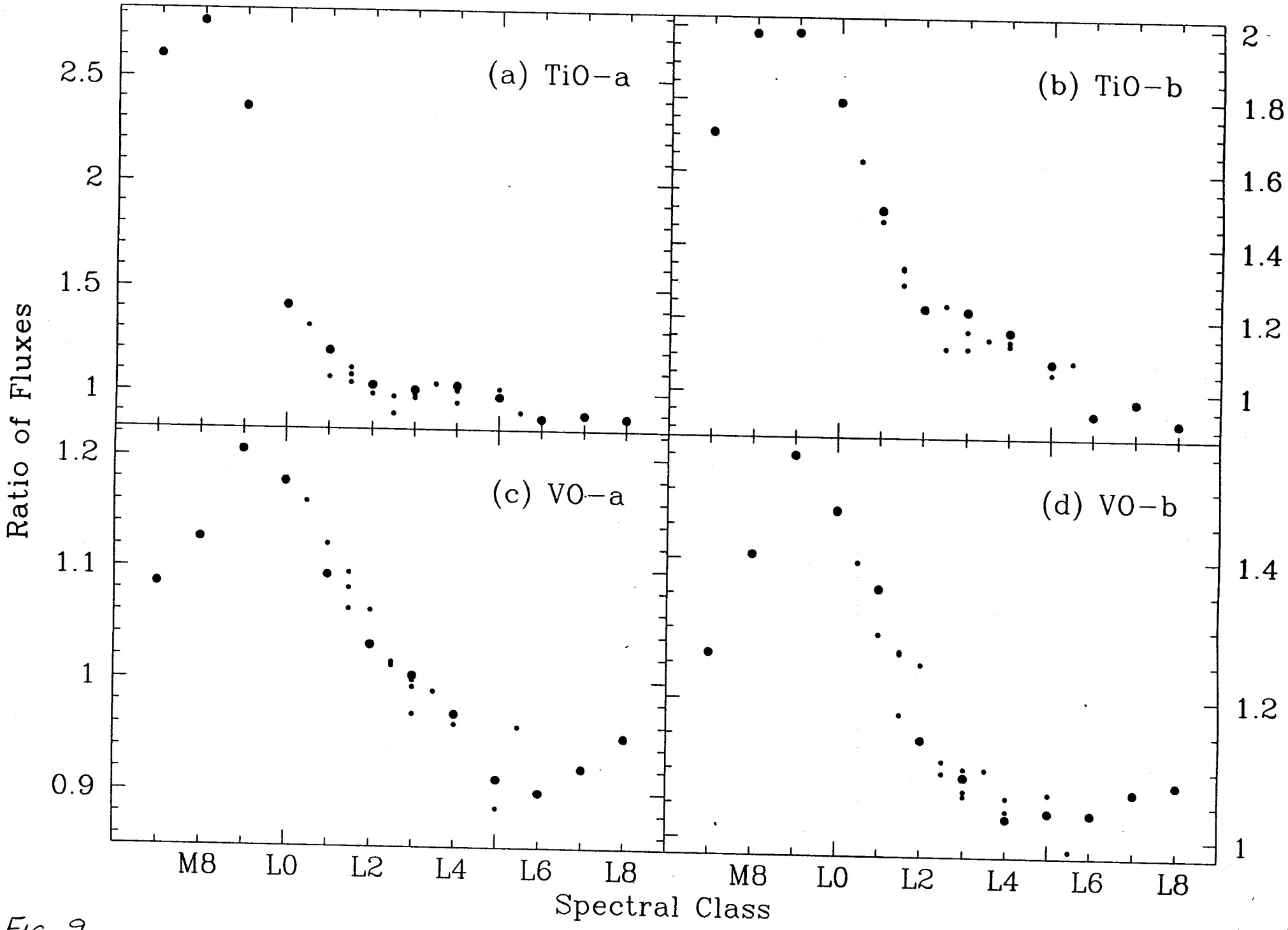
(a) TiO−a
(b) TiO−b
(c) VO−a
(d) VO−b
Ratio of Fluxes
Spectral Class
M8
L0
L2
L4
L6
L8
2.5
2
1.5
1
1.2
1.1
0.9
1.8
1.6
1.4

FIG. 9

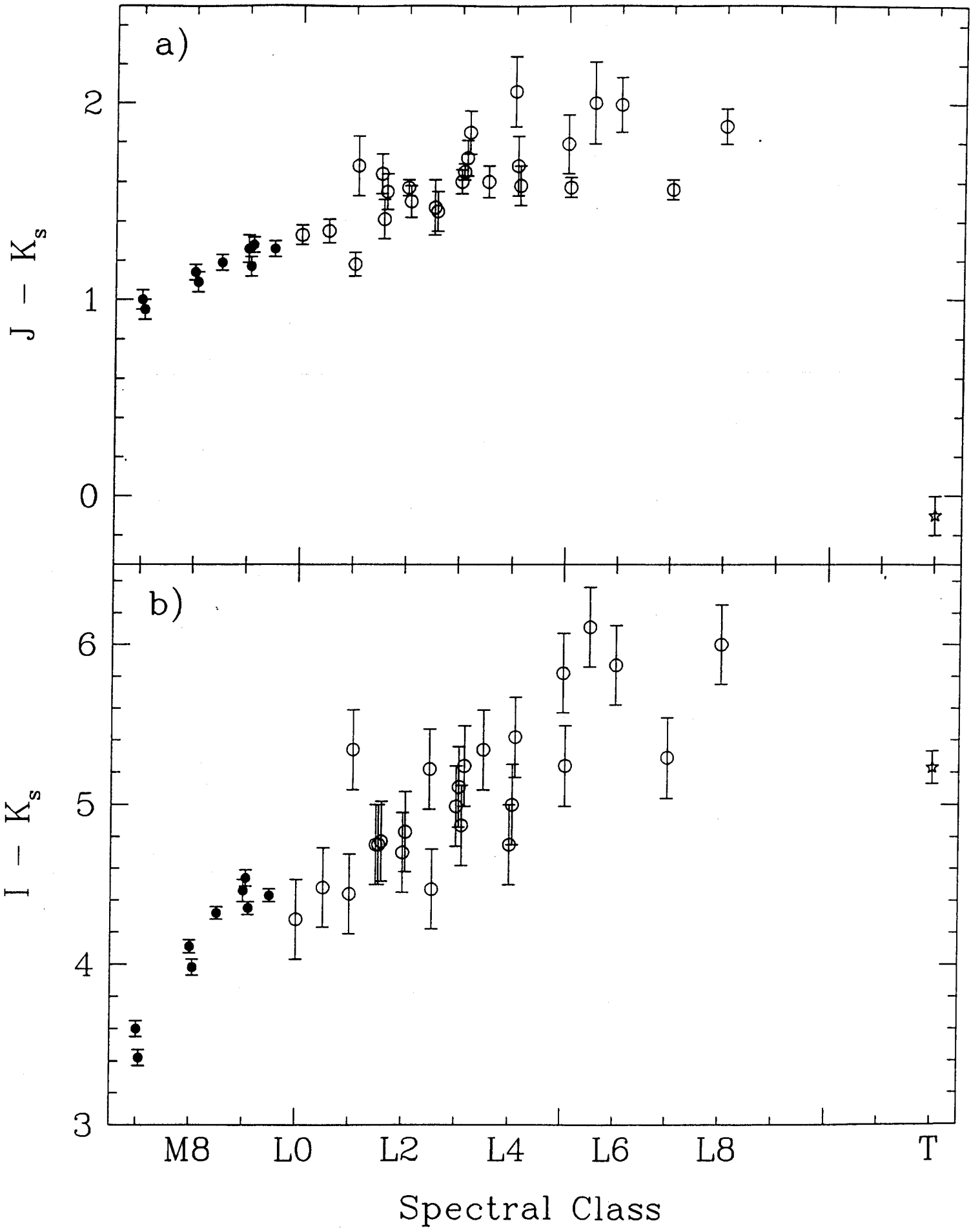

FIG. 13.

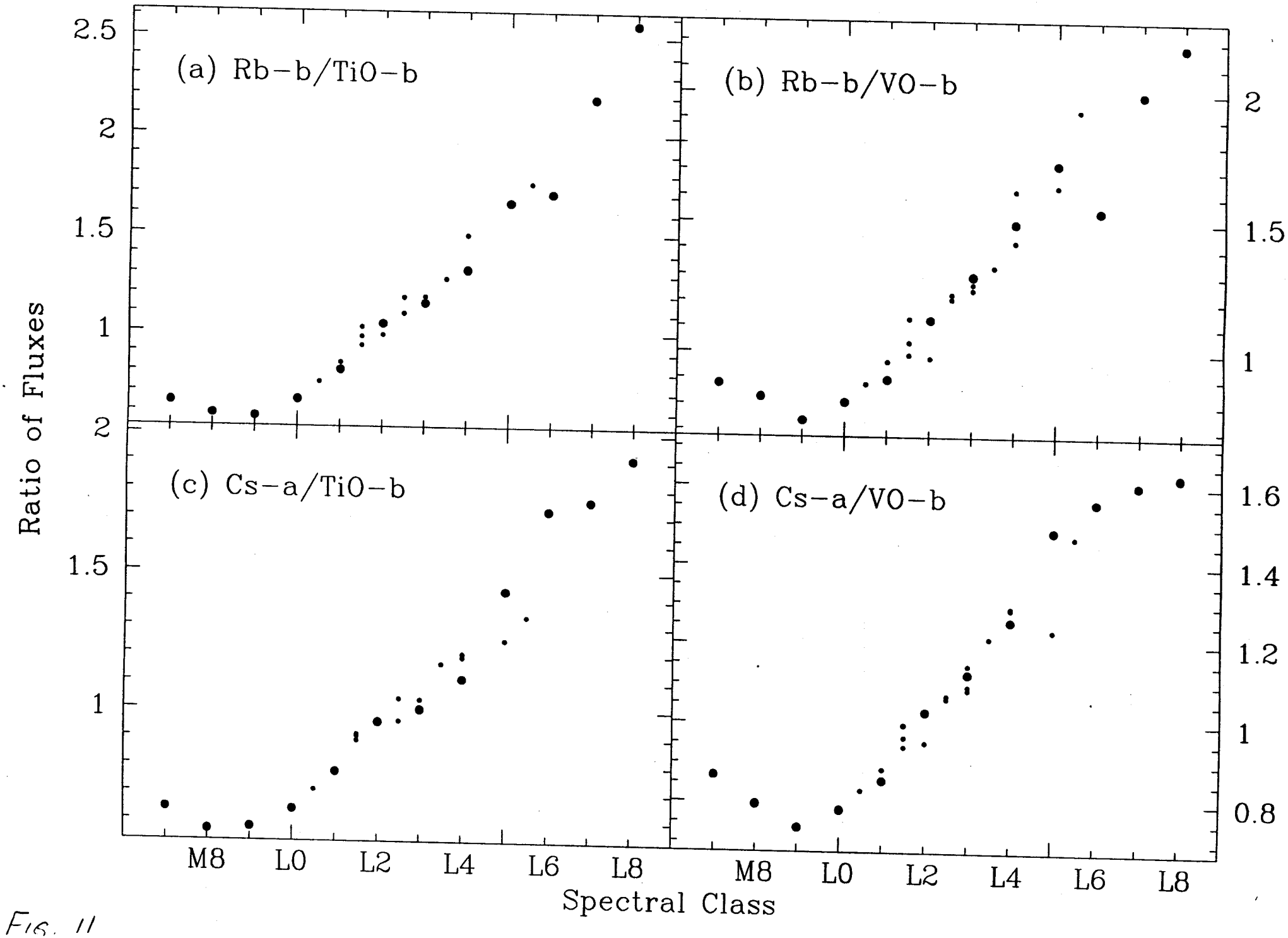
(a) Rb−b/TiO−b
(b) Rb−b/VO−b
(c) Cs−a/TiO−b
(d) Cs−a/VO−b
Ratio of Fluxes
Spectral Class
M8
L0
L2
L4
L6
L8
2.5
2
1.5
1
2
1.5
1
1.5
1
1.6
1.4
1.2
1
0.8

FIG. 11

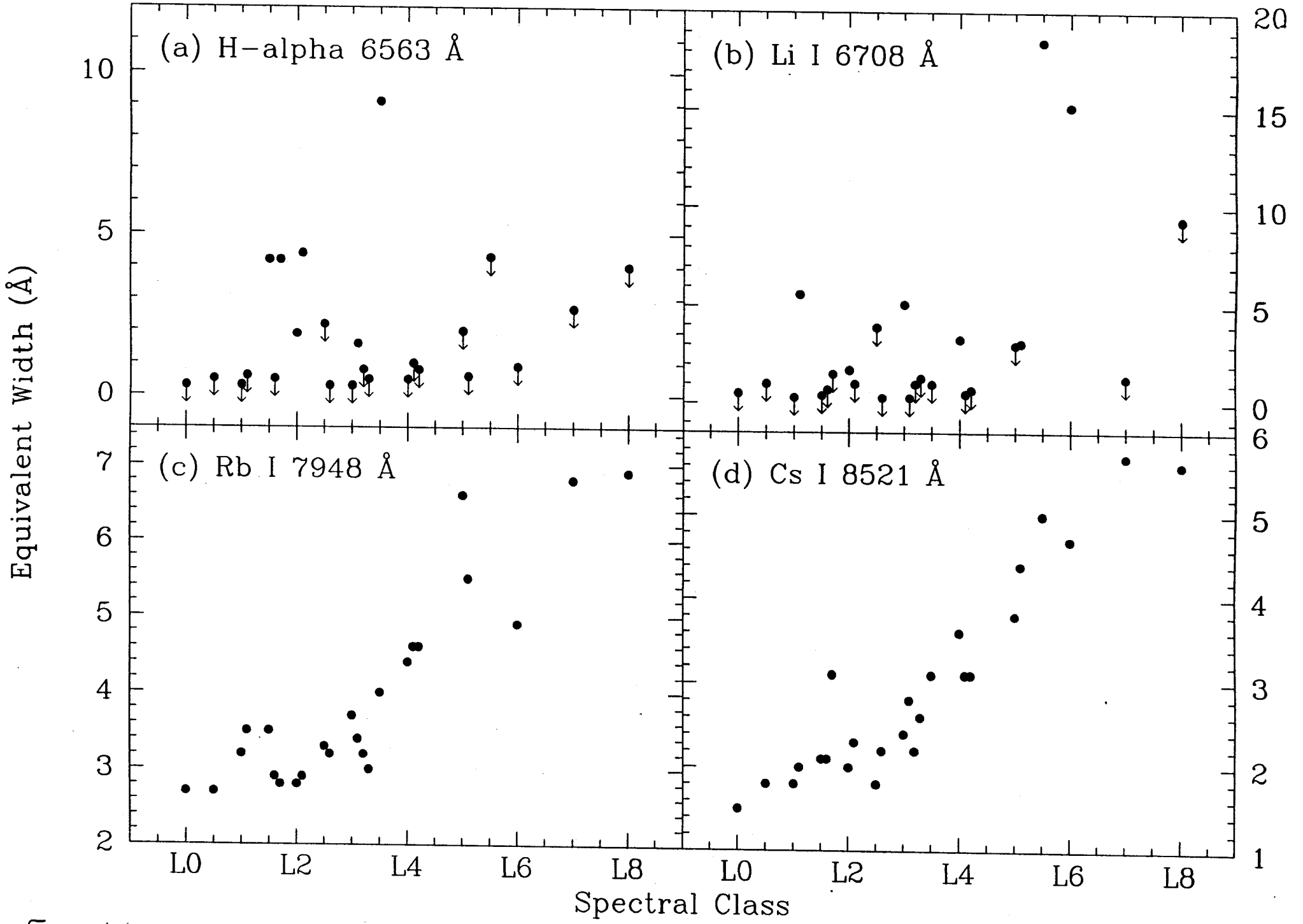
(a) H-alpha 6563 Å
(b) Li I 6708 Å
(c) Rb I 7948 Å
(d) Cs I 8521 Å
Equivalent Width (Å)
Spectral Class
L0
L2
L4
L6
L8
0
5
10
15
20
1
2
3
4
6
7

FIG. 15

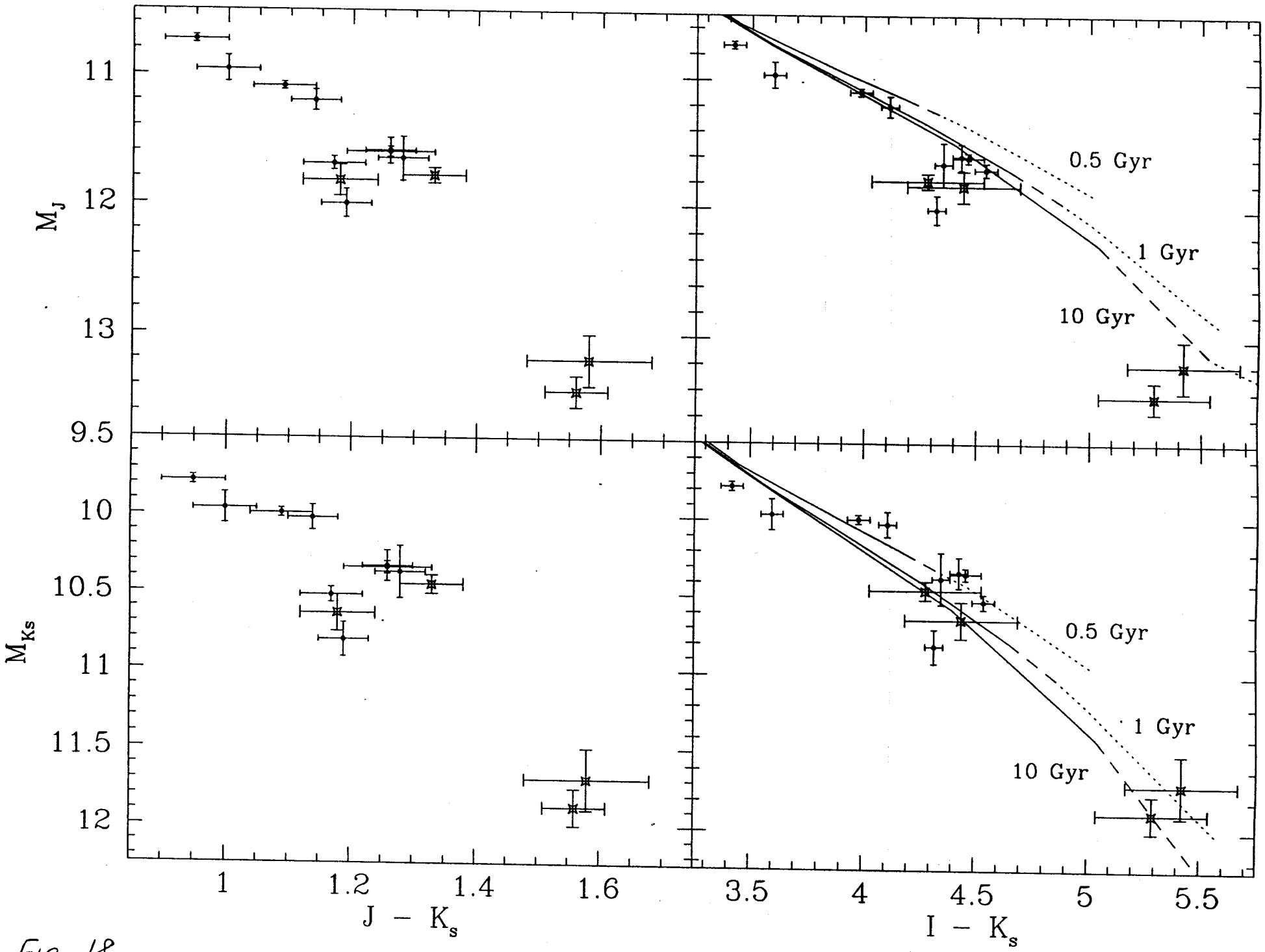
11
12
13
9.5
10
10.5
11
11.5
12
M_J
M_{Ks}
0.5 Gyr
1 Gyr
10 Gyr
0.5 Gyr
1 Gyr
10 Gyr
1
1.2
1.4
1.6
3.5
4
4.5
5
5.5
J − K_s
I − K_s

FIG. 18.